Proceedings of the Combustion Institute 40 (2024) 105620

Contents lists available at ScienceDirect

Proceedings of the Combustion Institute

journal homepage: www.elsevier.com/locate/proci

The role of C_3 and C_4 species in forming naphthalene in counterflow diffusion flames

Maximilian Hellmuth *, Raymond Langer, Anita Meraviglia, Joachim Beeckmann, Heinz Pitsch

Institute for Combustion Technology, RWTH Aachen University, Templergraben 64, 52056 Aachen, Germany

ARTICLE INFO

Keywords:
Counterflow diffusion flame
Speciation measurement
Allene
1-Buten-3-yne (C_4H_4, vinylacetylene)
Naphthalene

ABSTRACT

Allene and 1-buten-3-yne (C_4H_4) represent important intermediates in forming polycyclic aromatic hydrocarbons and soot. Hydrogen abstraction from allene provides the resonance-stabilized propargyl radical fueling molecular growth kinetics. However, the kinetics associated with 1-buten-3-yne and its involvement in the formation and growth of aromatics still need to be fully understood. One of the challenges is the complexity of the relevant chemistry in most combustion environments, which includes fuel-specific reactions in addition to reactions of C_4 species. This work attempts to simplify the relevant chemistry by using 1-buten-3-yne as fuel for the first time in counterflow diffusion flames. A pure allene and a 75/25 mol % allene/1-buten-3-yne blend flame were examined using gas chromatography–mass spectrometry and time-of-flight mass spectrometry. The boundary and operating conditions feature close equilibrium temperature, stoichiometric mixture fraction, and strain rate, allowing a meaningful kinetic comparison between the flames. Speciation data from both instruments were consistent for the vast majority of the species. The experimental results were compared to simulations performed with an updated, extensively validated, detailed chemical kinetic model. Notably, adding 1-buten-3-yne to the fuel reduced benzene and increased the formation of naphthalene. This showcases that the availability of C_3 and C_4 species impacts the kinetics of the two species differently. Pathway analyses revealed that benzene formation highly depends on C_3 species, while naphthalene relies on C_3 and C_4 species. Naphthalene formation depends on the abundance of 1,3-butadiyne (C_4H_2) and proceeds mainly via the $C_4 + 2\,C_3$ and $2\,C_3 + C_4$ pathways. Other pathways, such as HACA and phenyl radical-addition to C_4H_4, exhibited a minor impact. The present work highlights that uncertainties in the C_4H_2-related chemistry are highly relevant for the modeling of aromatics and may affect naphthalene predictions. Therefore, the experimental data of this study will provide a unique validation target for future kinetic model development.

1. Introduction

Allene (A-C_3H_4) and 1-buten-3-yne (C_4H_4) are important intermediates in the formation of polycyclic aromatic hydrocarbons (PAH) and soot. Hydrogen (H) atom abstraction from allene forms the resonance-stabilized propargyl radical (C_3H_3), an essential component in molecular growth kinetics [1–3]. The recombination of two propargyl radicals is the dominant source of the first aromatic ring within most combustion environments [4,5]. Recent studies also suggest that propargyl radicals are involved in several other molecular growth pathways producing larger aromatic species, e.g., naphthalene (A_2) via the recombination of fulvenallenyl (C_7H_5) and propargyl radicals [1–3,6,7].

While it is well-established that allene chemistry plays a vital role in forming aromatic compounds, the chemistry of 1-buten-3-yne, and its role in molecular growth pathways remain to be clarified. On the one hand, C_4H_4 may contribute directly to aromatics formation, for example, through reactions with propargyl radicals [8,9], benzyne (O-C_6H_4) [10], and phenyl radicals (A_1-) [11]. On the other hand, reactions of C_4H_4 may indirectly affect aromatics' formation. Of central importance are the H-atom abstraction from C_4H_4 and subsequent decomposition of the formed C_4H_3 species, which produce 1,3-butadiyne (C_4H_2). Several recent kinetic modeling studies [1–3,6,7] suspect C_4H_2 to be a crucial species in forming naphthalene. These studies [1–3,6,7] showed consistently that the formation of naphthalene mostly bypasses benzene (A_1) and instead proceeds via fulvenallenyl radicals according to the following two-step mechanism:

1. $C_4H_2 + C_3H_3 \rightleftharpoons C_7H_5$,
2. $C_7H_5 + C_3H_3 \rightleftharpoons A_2$.

The above naphthalene formation mechanism, referred to as the $C_4 + 2\,C_3$ pathway in the following, was found to be the dominating

* Corresponding author.
E-mail address: m.hellmuth@itv.rwth-aachen.de (M. Hellmuth).

https://doi.org/10.1016/j.proci.2024.105620
Received 5 December 2023; Accepted 2 July 2024
Available online 31 July 2024

source of naphthalene in the combustion of various hydrocarbons [1–3] and bio-hybrid fuels [6,7]. However, despite the suspected significance, validation remains difficult due to numerous sources of uncertainty potentially affecting model predictions:

1. Uncertainties in the reactions of the $C_4 + 2\,C_3$ pathway are large, especially the second step, modeled in analogy to the self-recombination of propargyl radicals [4]. Recent experimental and theoretical work [12] confirmed the viability of the second step, but the quantitative rate coefficient determinations remain unavailable.
2. The sensitivity analysis performed by Langer [13] suggests that uncertainties in fuel-specific reactions may strongly impact naphthalene predictions. For example, uncertainty in several reactions from the C_2 chemistry may contribute to naphthalene prediction errors in ethylene (C_2H_4) counterflow flames [13].
3. The frequently seen large deviations [3,6,14] between measured and predicted C_4H_2 mole fractions hamper the analysis of the $C_4 + 2\,C_3$ pathway.

The reason for the poor C_4H_2 predictions is the high uncertainty in several potential formation pathways of dehydrogenated C_4 components and their oxidation chemistry [13]. For most fuels, the following reactions can contribute to the formation of C_4 species [3]:

1. $C_2H_2 + C_2H \rightleftharpoons C_4H_2 + H$,
2. $C_2H_4 + C_2H \rightleftharpoons C_4H_4 + H$,
3. $C_2H_4 + C_2H_3 \rightleftharpoons C_4H_6 + H$.

Several H-atom abstraction and decomposition reactions facilitate the interconversion from 1,3-butadiene (C_4H_6) and C_4H_4 to C_4H_2.

The present work attempts to circumvent most of the complexities involved with the formation of C_4 species, thereby facilitating the analysis of the $C_4 + 2\,C_3$ pathway. The chemical structures of a pure allene and an allene/1-buten-3-yne blend flame were studied in a counterflow configuration. Selecting allene as the primary fuel component in both flames ensured high availability of propargyl radicals. The 1-buten-3-yne substitution emphasizes the chemical effect of adding a dehydrogenated C_4 species as a fuel component, where the way of substitution preserved the similarity of the temperature time history between the two flames.

Introducing 1-buten-3-yne as a fuel component has several advantages. To the authors' knowledge, this is the first work to investigate the oxidation chemistry of 1-buten-3-yne in a flame, which makes the flame structure data a unique target for kinetic model validation. Introducing 1-buten-3-yne as a fuel component simplifies the relevant formation pathways of C_4H_2. In addition, the high availability of 1-buten-3-yne offers the possibility of investigating the relevance of C_4H_4-based molecular growth pathways, e.g., H-abstraction-vinylacetylene-addition (HAVA) [11,15].

2. Experimental and computational methods

Our counterflow burner setup is comprehensively described in [16]. In summary, the two opposed nozzles were $L = 10\,\text{mm}$ apart and had a diameter of 20 mm. The fuel diluted with argon (Ar) was supplied through the upper nozzle (fuel side), while oxygen (O_2) and Ar were introduced through the lower nozzle (oxidizer side). The fuel nozzle and its associated line were heated to 353 K. A co-flow of nitrogen protected the oxidizer and fuel streams from the surrounding environment.

Speciation data were obtained using gas chromatography–mass spectrometry (GC–MS) and time-of-flight mass spectrometry (ToF–MS). Only the key information is given here since a detailed description of our setups and methodology is documented elsewhere [6,16,17]. Since both methods involve intrusive probing of the flames, photos were taken with a camera (Canon EOS 1200D) during the sampling process to evaluate the probes' position and impact on the flames. The spatial uncertainty was estimated to be within ±0.4 mm for both devices.

For the GC–MS [6,17], a ceramic sampling capillary with an inner/outer diameter of 0.2/0.5 mm was used to extract gaseous samples at high spatial resolution at minimal flame perturbation. A storage unit conserved the gaseous samples at 473 K.

Analysis was performed by a gas chromatograph (GC) equipped with a mass-selective detector (MSD), thermal conductivity detector (TCD), and flame ionization detector (FID). The TCD quantified hydrogen (H_2), carbon monoxide (CO), and carbon dioxide (CO_2), while hydrocarbons up to C_{10} were identified and quantified by the MSD and FID, respectively. Species up to C_7 were calibrated using gaseous standards of known compositions, and from C_6 to C_{10} using the cold-gas sampling of a self-prepared mixture evaporated in a hot stream of Ar. We used species calibrated by both methods, e.g., benzene, to assess our calibration quality, yielding only a minor change in the calibration factors. We estimate the uncertainty in the peak mole fraction of directly calibrated species to range from ±1 % to ±15 %, including the uncertainty estimates from calibration and repeatability. The effective carbon number (ECN) approach [18,19] was used for quantification if there was no calibration standard available. A test with directly calibrated species indicated an additional uncertainty of ±25 % for the ECN approach, making the estimated uncertainty in the peak mole fraction of these species range from ±28 % to ±37 %.

For the ToF-MS [16], species were sampled using a quartz probe with an inner/outer diameter of 0.03/1 mm. They then undergo three different pressure stages to form a molecular beam, which leads to an aerodynamic quench of the reactions, conserving the sample composition. Once the molecules reach the ionization chamber, they are ionized by electrons of defined energy, accelerated into the flight tube by a two-stage ion extraction section, and reflected by a double-stage reflectron until they reach the detector. Since the molecules are accelerated differently based on their mass and ionization, their flight times also vary. The detector is a multichannel plate, and the flight times are recorded with a multichannel scaler. The mass resolution $\Delta m/m$ is ≈4000. 17 eV electrons were used for ionization.

Many factors such as probing effects, molecular fragmentation, and assumptions about the quantification process impact the data evaluation. Therefore, the uncertainty is estimated to be ±15 % for the fuels, O_2, H_2, CO, CO_2, and Ar [16]. An undesired water background, comparable in magnitude to the water generated during the combustion process, was detected in the ToF due to condensation on the ionization chamber walls. Therefore, we estimate a factor 2.5 of uncertainty in the water quantification. The uncertainty of directly calibrated intermediates is ±30 %. If the calibration factor was obtained using indirect methods, it amounts to a factor of two to three.

Langer et al. [3,13] recently published a detailed chemical kinetic model including all the molecular growth pathways discussed in the introduction. This kinetic model was used to perform simulations with FlameMaster [20] after introducing one update. Previously performed sensitivity analyses [13] revealed that predictions of substituted monoaromatic species may be sensitively affected by a relatively crude description of reactions of C_3H_3 and C_4H_4. Hence, the comprehensive kinetics on the C_7H_7 potential energy surface investigated by Martí et al. [9] were incorporated into the model for the flame structure analysis. The updated kinetic model reflects the state-of-the-art understanding of PAH chemistry, building on numerous prior theoretical, experimental, and modeling studies [3,13]. The CHEMKIN input files for the revised model and a species dictionary are provided in the supplementary material SM-1. The species dictionary provides molecular identifiers and structural formulas, which can also be consulted to understand species names introduced in the manuscript. Additionally, Fig. S1 in SM-2 compares measured and predicted peak mole fractions for 31 additional counterflow flow flames covering multiple fuels and a broad pressure range. The revised model predicts most aromatics up to the size of C_{12} species with an average deviation of a factor of two from experimental measurements. Validation targets sensitive to oxidation chemistry remain unaffected by the revision, and the reader is referred

to the authors' prior work for comprehensive validation with data from 79 publications [3,13].

Ensuring flame comparability and reducing the differences to solely chemical effects is imperative to studying the impact of fuel composition on chemical kinetics. As outlined in our previous work [6,7], we achieve this by keeping the global strain rate $a = (4|u_2|)/L$, the stoichiometric mixture fraction $Z_{st} = 1/(1 + \nu Y_{F,1}/Y_{O_2,2})$, and the equilibrium flame temperature (T_{eq}) at the location of Z_{st} close. u_2 is the velocity of the oxidizer flow, ν is the stoichiometric mass ratio of oxygen to fuel, and $Y_{F,1}$ and $Y_{O_2,2}$ are the fuel and oxygen mass fraction in the fuel and oxidizer flow, respectively. The result is a similar temperature time history (see Fig. S2 in SM-2), which preserves species' self-similarity. The differences in computed T_{eq} and maximum flame temperature of the two flames are 2 K and 17 K, respectively. Both flames were laminar diffusion flames and stabilized on the fuel side of the gas stagnation plane with $Z_{st} = 0.510$. The strain rate was set to $60\,s^{-1}$, and momentum balance was imposed on the flows, leading the theoretical gas stagnation plane to position in the middle of the two nozzles. Two flames were investigated in this study: a pure allene flame (C_3 flame) with a fuel and oxygen mole fraction of 5 % and 20 %, respectively, and a 1-buten-3-yne-substituted flame (C_3+C_4 flame) with a fuel and oxygen mole fraction of 4.7 % and 19.9 %, respectively. In the latter, the fuel was composed of 75 mol % A-C_3H_4 and 25 mol % C_4H_4. Allene and 1-buten-3-yne were acquired as gas mixtures from Air Products GmbH: 10 mol % A-C_3H_4 in Ar and 3 mol % C_4H_4 in Ar. An analysis of both mixtures using our GC-MS revealed several impurities in the fuel mixtures. The largest impurity was H_2, with approximately 0.175 mol % in the C_3+C_4 flame. All impurities included in the kinetic model [3,13] were accounted for in the simulations. A comparison of simulation results with and without the detected impurities indicated no change in the flame structure and negligible effects on the species' peak mole fractions. Tables S1-S3 in SM-2 detail the boundary conditions, including the impurities. Monte Carlo simulations indicated that the uncertainty estimates in the experimental mole fractions, Z_{st}, and a are below 2.0 %. Details on the evaluation are given in SM-2.

3. Results and discussion

Figs. 1–3 show the spatial mole fraction profiles of selected species. The fuel flow enters from the left, and the oxidizer flow enters from the right. The zero position of the spatial coordinate z denotes the theoretical gas stagnation plane. Profile broadening of the experimental data observed in Fig. 1 and especially in the region of steep gradients in Figs. 2 and 3 may be a probing artifact, limiting spatial resolution to a certain extent [6,16]. Further, the spatial shift of the ToF compared to the GC data on the fuel side in Figs. 1–3 may root in the different nozzle sizes of the instruments impacting the flow field and the flame differently. In this region, the impact of the intrusive probe is most pronounced [21]. Therefore, we mainly focus on comparing the peak mole fractions in the following, an approach used successfully in previous kinetic modeling studies [3,6,7,22].

3.1. Major species

Fig. 1 shows the spatial mole fraction profiles of the reactants and major intermediates/products. Replacing 25 mol % of allene with 1-buten-3-yne leads to no considerable change in the species' mole fraction profiles. The GC and ToF datasets align, and the kinetic model simulations lie within the experimental uncertainty for most species. The carbon count for the GC data set given in Fig. S3 in SM-2 indicates overall good carbon recovery for both flames. Therefore, the deviation in peak mole fraction for carbon monoxide (Fig. 1(d)) and acetylene (C_2H_2, Fig. 1(f)) may come from the carbon remaining in the fuel molecules (Fig. 1(a) and Fig. 1(b)) at this position. The same holds for carbon dioxide (Fig. 1(c)) in the C_3+C_4 flame. A similar observation was made in two of our previous studies [6,7].

3.2. Intermediate species

Moving on to C_1–C_4 intermediates featured in Fig. 2, one can see the advantage of using two measurement instruments in this study. While the ToF cannot resolve the C_3H_4 isomers allene and propyne (P-C_3H_4, Fig. 2(c)), the GC can achieve this. In the ToF spectrum, C_4H_6 was taken as 1,3-butadiene (Fig. 2(f)), while the GC detected three additional C_4H_6 isomers, e.g., 1,2-butadiene (12-C_4H_6, see Fig. S5(b) in SM-2). On the other hand, the GC could not quantify 1,3-butadiene for the C_3+C_4 flame since the peak of 1-buten-3-yne covered it. A similar overlap existed for 1,3-butadiyne (Fig. 2(e)) in the ToF spectrum, where the fragments of 1-buten-3-yne covered the signal of 1,3-butadiyne in the C_3+C_4 flame. Despite these instrument-specific challenges, a profile could be obtained for each species in each flame presented in this study by either the GC or the ToF. For the cases in which a GC and ToF dataset exists in Fig. 2, most measured species peak mole fractions agree within the experimental uncertainty.

The kinetic model simulations correctly capture the trends for most species in Fig. 2, while several quantitative discrepancies exist. Methane (CH_4, Fig. 2(a)) is overpredicted by a factor of 1.4. Kukkadapu et al. [1] observed an even higher overprediction in a similar allene counterflow diffusion flame. Since methyl radical (CH_3)-driven H-atom abstraction from propyne (Fig. 2(c)) is the primary source of methane, it decreases in the C_3+C_4 flame. For ethylene (Fig. 2(b)), there is a quantitative and qualitative agreement between the ToF and the kinetic model simulations. The GC generally detects less ethylene and indicates a decrease in peak mole fraction when adding 1-buten-3-yne. This is the only case in Fig. 2 where the experimental peak mole fraction differences exceed the instruments' uncertainties. Nevertheless, the discrepancy is marginal. Propyne (Fig. 2(c)) originates almost entirely from the isomerization of allene in our flame environments. Consequently, a reduction in allene leads to a decrease in propyne peak mole fraction. Since the C_3 chemistry received much attention during the last few years [23], the overprediction of propyne in allene-based flames is unexpected, and a revisit may be needed. Propene (C_3H_6, Fig. 2(d)) forms in fewer amounts than it is added as a fuel impurity in both flames. The lack of a direct calibration of C_3H_6 in the ToF may explain the quantitative discrepancy to the GC dataset, which is a factor of 1.6 for both flames. The kinetic model simulations severely overpredict 1,3-butadiyne (Fig. 2(e)) by a factor of three in the C_3 flame. While the large uncertainty in the C_4H_2 chemistry is well-documented [3,6,7,13,14], surprisingly, the overprediction becomes especially pronounced in the C_3+C_4 flame, where the formation of C_4H_2 from C_4H_4 is relatively simple (H-atom abstraction from C_4H_4 and subsequent decomposition of C_4H_3 species). As discussed in Section 3.3, the observed overprediction by up to a factor of six is highly relevant for the formation of aromatic species, and the C_4H_2 chemistry needs more attention in future model development. 1,3-butadiene (Fig. 2(f)) is formed more than it is added as fuel impurity in the C_3+C_4 flame. Contrary to the other species shown in Fig. 2, it is slightly underpredicted. However, the model captures the decrease in the C_3+C_4 flame observed in the ToF dataset. According to a rate of production (ROP) analysis for the C_3 flame (C_3+C_4 flame), the recombination of methyl and propargyl radicals forms the majority of 1,3-butadiene via the isomerization of 1,2-butadiene (see Fig. S5(b) in SM-2) with 47 % (51 %) or directly with 13 % (11 %). The kinetic model simulations similarly match 1,2-butadiene compared to 1,3-butadiene. Another source of 1,3-butadiene is the oxidation of 1,3-cyclopentadiene (C_5H_6, see Fig. S6(b) in SM-2) with 30 % (both flames). More C_2 to C_4 species are summarized in Fig. S5 in SM-2. The simulations match the trends, and quantitative discrepancies are similar to those reported in Fig. 2.

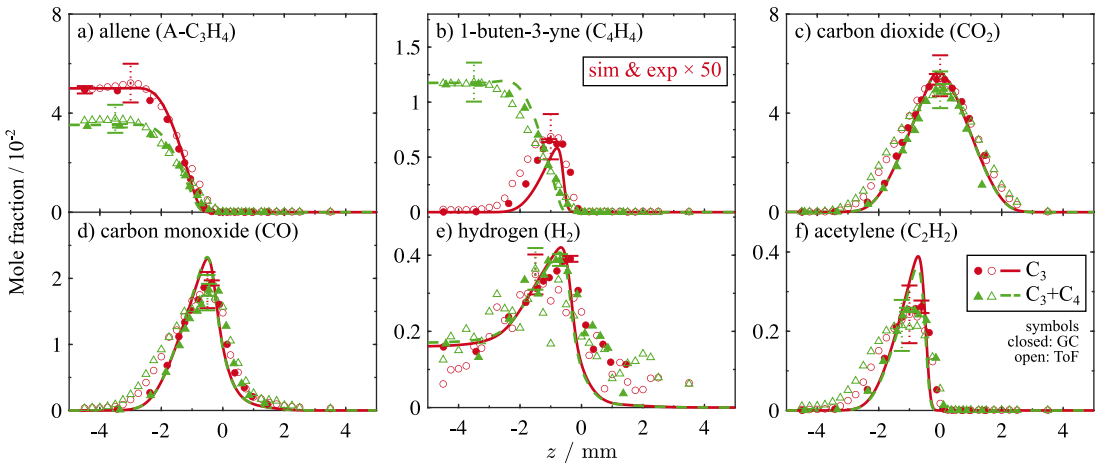

Fig. 1. Measured (symbols) and computed (lines) mole fraction profiles of the reactants and major intermediates/products as a function of distance from the theoretical gas stagnation plane. Closed symbols represent the GC data. Open symbols represent the ToF data. Red dots and solid lines denote the C_3 flame, and green triangles and dashed lines denote the C_3+C_4 flame. Colored error bars indicate the experimental uncertainty in the mole fraction (GC: solid line, ToF: dotted line). The spatial uncertainty for both devices is within ±0.4 mm. (For interpretation of the references to color in this figure legend, the reader is referred to the web version of this article.)

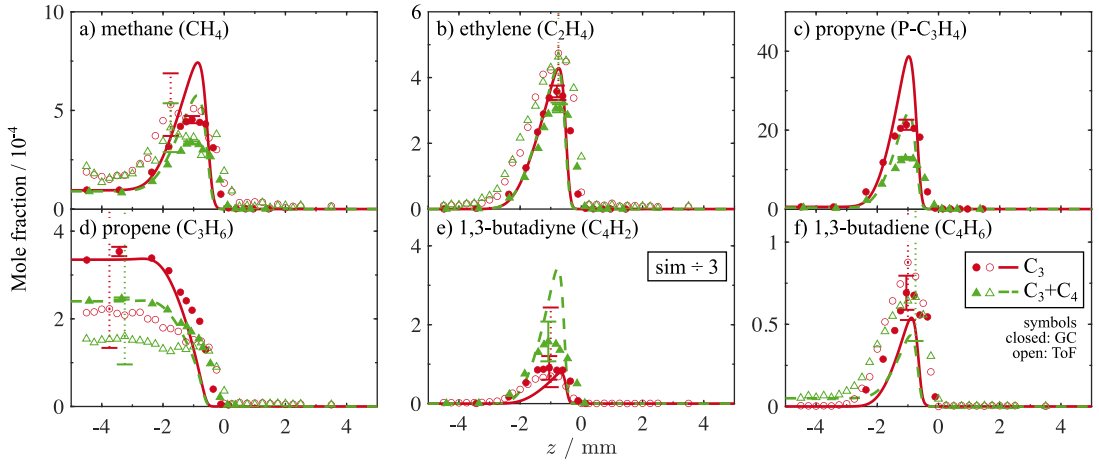

Fig. 2. Measured (symbols) and computed (lines) mole fraction profiles of selected C_1–C_4 intermediates as a function of distance from the theoretical gas stagnation plane. Closed symbols represent the GC data. Open symbols represent the ToF data. Red dots and solid lines denote the C_3 flame, and green triangles and dashed lines denote the C_3+C_4 flame. Colored error bars indicate the experimental uncertainty in the mole fraction (GC: solid line, ToF: dotted line). The spatial uncertainty for both devices is within ±0.4 mm. (For interpretation of the references to color in this figure legend, the reader is referred to the web version of this article.)

3.3. Aromatic species

Turning to the aromatic species shown in Fig. 3, the GC and ToF datasets agree within the experimental uncertainties, and particularly well for phenylethyne (A_1C_2H, Fig. 3(c)), indene (C_9H_8, Fig. 3(e)), and naphthalene (Fig. 3(f)). In the C_3+C_4 flame, the GC could not quantify styrene and phenylethyne since xylenes (see Figs. S6(i) and S6(j) in SM-2) as fuel impurities eluted at the same time.

The kinetic model simulations replicate the trends exhibited by the experiments for the species shown in Fig. 3, except for toluene (A_1CH_3, Fig. 3(b)) and phenylethyne (Fig. 3(c)). Similar to the C_1–C_4 intermediates (Fig. 2), there is a consistent overprediction of at least a factor of two. An exception is styrene (Fig. 3(d)). As expected, benzene's (Fig. 3(a)) peak mole fraction decreases at the partial substitution of allene with 1-buten-3-yne since the major propargyl radical (see Fig. S7 in SM-2) producers, allene and propyne, which fuel the C_3 + C_3 pathways [6,24], are reduced. A replacement of these pathways by C_4-based pathways was not observed. A ROP analysis of the C_3+C_4 flame revealed that C_4H_4 – in contrast to C_4H_6 – cannot readily form the resonance-stabilized I-C_4H_5, which may promote A_1 formation via I-C_4H_5 + C_2H_2 ⇌ A_1 + H [25]. For both flames, the kinetic model overpredicts the benzene peak mole fraction by up to a factor of four, which is significantly larger than the average deviation of only 1.8 shown in Fig. S1 in SM-2 for various other fuels. As predictions of aromatic species, such as benzene, are highly sensitive to the fuel-specific chemistry [3], uncertainties in the allene-specific chemistry adopted from the model developed by Panigrahy et al. [23] are likely the reason for benzene overprediction. This observation is in line with the notable discrepancies for propyne (Fig. 2(c)), which were discussed earlier. Addressing benzene overpredictions in the investigated flames is beyond the scope of this work and should be targeted by future kinetic studies. The C_1- and C_2-substituted monocyclic aromatics do not react uniformly to the addition of C_4H_4. While the notable increase for toluene (Fig. 3(b)) and the slight increase for styrene (Fig. 3(d)) in the experimental peak mole fractions are not captured, the decrease in the peak mole fraction of phenylethyne (Fig. 3(c)) is not as distinct in the experiments as depicted in the kinetic model simulations. Indene (Fig. 3(e)) is little affected by the larger availability of C_4 species in the species pool. In contrast to benzene, naphthalene (Fig. 3(f)) formation is promoted significantly in the C_3+C_4 flame, highlighting that both species depend differently on the availability of C_3 and C_4 species. However, the extent differs by about a factor of two between the experiments and the simulations, which may be traced back to the overprediction of C_4H_2 and is discussed later. Fig. S6 in SM-2

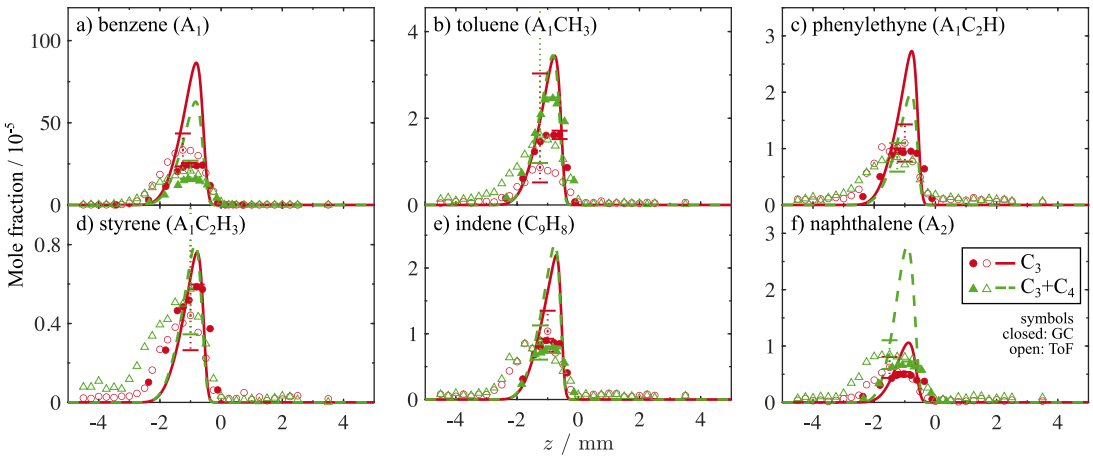

Fig. 3. Measured (symbols) and computed (lines) mole fraction profiles of selected mono- and polycyclic aromatic species as a function of distance from the theoretical gas stagnation plane. Closed symbols represent the GC data. Open symbols represent the ToF data. Red dots and solid lines denote the C_3 flame, and green triangles and dashed lines denote the C_3+C_4 flame. Colored error bars indicate the experimental uncertainty in the mole fraction (GC: solid line, ToF: dotted line). The spatial uncertainty for both devices is within ±0.4 mm. (For interpretation of the references to color in this figure legend, the reader is referred to the web version of this article.)

shows more quantified linear and monocyclic hydrocarbons ranging from C_5 to C_8. 1,3-Cyclopentadiene (C_5H_6, see Fig. S6(b) in SM-2) and ethylbenzene ($A_1C_2H_5$, see Fig. S6(h) in SM-2) are overpredicted by a factor of two and 2.7, respectively. In the C_3+C_4 flame, the model correctly predicts the increase of 1,3-cyclopentadiene and the consumption of ethylbenzene as an impurity.

We elaborate on the kinetics of the species depicted in Fig. 3 by performing reaction pathways analyses based on the methodology of Hellmuth et al. [6]. A rate of production analysis provided the net flux for each pathway. If there was a considerable flux between the stable species and its radicals, they were treated as one. All pathways discussed in the following are included in the kinetic model provided in SM-1.

Fig. 4 presents a simplified scheme of C_1- and C_2-substituted monocyclic aromatics and indene formation in both investigated flames. Due to the rich supply of C_3 species, they dominate the primary formation pathways. The C_4 chemistry does not shape the formation of C_2-substituted aromatics and indene, which the minor changes in mole fraction profiles of these species in Fig. 3 confirm. Indene formation occurs through ring closure after the recombination reaction of C_3H_3 and phenyl radicals and the C_3H_3-addition to benzyne. The latter is closely linked to the production of toluene, as will be discussed later. Most studies do not report data for benzyne. Therefore, we included its mole fraction profiles in Fig. S6(e) in SM-2 showcasing the simulations' quantitative agreement within the experimental uncertainty. The oxidation of indene is a major source of C_2-substituted aromatics. Initially, styrene is formed, which then undergoes H-atom addition and elimination, producing ethylbenzene and phenylethyne, respectively. Mebel et al. [11] investigated reactions of allene and phenyl radicals in theory-based computations, and Fig. 4 shows that the investigated pathways can contribute to phenylethyne formation via an intermediate adduct with a branched substitute. Since the experimental and computed trends for phenylethyne (Fig. 3(c)) deviate, the influence of this pathway may be overestimated in the model. In environments with lower availability of allene, it is usually not favored to the same extent [3].

Toluene depends on the C_4 chemistry, as evidenced by the increasing peak mole fraction in the experiments (Fig. 3(b)). The reaction network in Fig. 4 suggests that a rich supply of C_3 and C_4 species in the C_3+C_4 flame promotes the formation of C_7 species. The dominant channels in forming toluene in Fig. 4 were updated based on the work of Martí et al. [9]. Notably, compared to observations in our previous studies [6,7], the relevance of propargyl radical-addition to 1-buten-3-yne in forming toluene is reduced. While the introduced

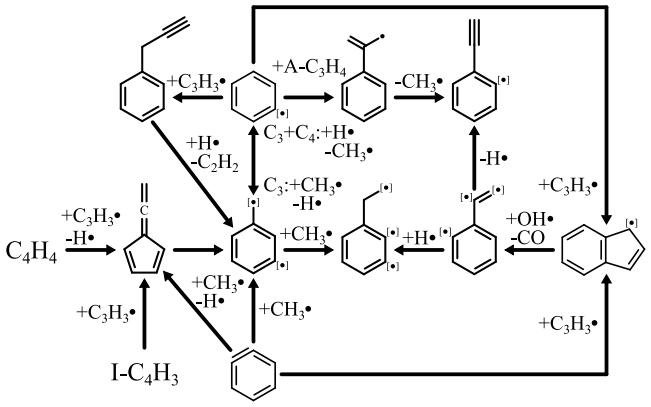

Fig. 4. Simplified reaction network of benzyne, benzene, fulvenallene, C_1- and C_2-substituted monocyclic aromatic species, and indene for both investigated flames. Dots in square brackets indicate potential radical sites.

kinetics [9] are expected to be more accurate, the more pronounced increase in toluene peak mole fractions in the experiments compared to the simulations (Fig. 3(b)) suggests that further revisions may be required in future work. The impact of the increased availability of C_4 species in the C_3+C_4 flame even results in the net flux reversal between benzene and toluene. Additionally, Fig. 4 illustrates the strong interconnection between toluene and ethylbenzene.

Fig. 5 shows the formation network of naphthalene, including pathways contributing more than 10 % to its formation. Three main channels were identified in both flames and are listed in descending order of contribution: (1) recombination reactions of C_3H_3 and fulvenallenyl radicals [1], (2) ring-enlargement initiated by the recombination of methyl and indenyl radicals [26], and (3) phenyl radical-addition to C_4H_2 [3]. The significance of pathways (1) and (2) was observed in several prior kinetic modeling studies [1–3,6,7]. Notably, the oxidation of phenylethyne, modeled in analogy to benzene oxidation, contributes to the fulvenallenyl radical formation. The third pathway is usually of minor importance for naphthalene formation [3] and may be specific to the investigated flame conditions. Pathways (1) and (3) depend on the poorly predicted abundance of C_4H_2, which underlines the high relevance of reducing the uncertainty in the related chemistry in future work. The classic H-abstraction-C_2H_2-addition (HACA) [27,28] affects naphthalene formation negligibly. Given the high availability of 1-buten-3-yne in the C_3+C_4 flame, it is interesting that

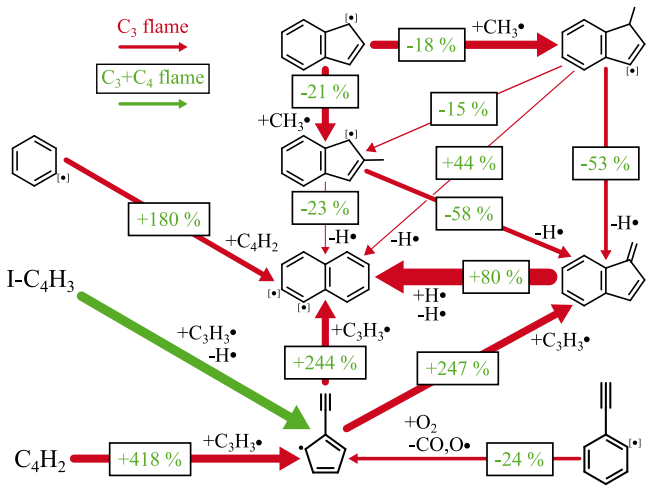

Fig. 5. Reaction pathway analysis for naphthalene. Dots in square brackets indicate potential radical sites. The arrow thickness corresponds to the net flux in the C_3 (red) and C_3+C_4 flame (green), respectively. Boxed numbers on each arrow indicate the change of net flux in the C_3+C_4 flame relative to the C_3 flame. (For interpretation of the references to color in this figure legend, the reader is referred to the web version of this article.)

phenyl radical addition to C_4H_4 (HAVA) [11,15], contributes only up to 7 % to naphthalene formation. The pathway is modeled based on the theoretical investigation of Mebel et al. [11], which suggests that naphthalene is produced via a two-step mechanism involving the formation of 1-phenylvinylacetylene. Due to the abundance of C_4H_4 in the C_3+C_4 flame, this pathway may be marginal in most other combustion environments.

The comparison of reaction fluxes in the C_3 and C_3+C_4 flame reveals which pathways are C_4-driven. Although there is little qualitative difference in the reaction pathways, the changes in the dominant reaction fluxes exceed −50 % and +400 %. C_4-driven pathways, whose net flux rises by adding C_4H_4, make up 83 % of total naphthalene formation in the C_3+C_4 flame. The main impact comes from the $C_4 + 2\,C_3$ pathway, contributing more than half of the net flux toward naphthalene. Here, 10 % comes from the recombination reaction of C_3H_3 and 1-butyl-3-yne radicals (I-C_4H_3) because 1-buten-3-yne as fuel provides I-C_4H_3 in large amounts. A part of the contribution from the pathway (2) shifts from benzofulvene to direct naphthalene formation due to the substantial increase in the net flux of fulvenallenyl radical toward benzofulvene. However, as the formation of naphthalene via ring-enlargement pathways requires no C_4 species, the net flux decreases overall. Pathway (3), phenyl radical-addition to C_4H_2, could be classified as a $2\,C_3 + C_4$ pathway, and is, in essence, a variant of the $C_4 + 2\,C_3$ pathway. This pathway is boosted and provides 20 % of the overall naphthalene formation in the C_3+C_4 flame.

4. Conclusions

We performed an experimental and numerical study on the role of C_3 and C_4 species in forming naphthalene. Two counterflow diffusion flames were probed using GC–MS and ToF–MS to obtain a rich species dataset. A close equilibrium temperature and the same stoichiometric mixture fraction, $Z_{st} = 0.510$, and strain rate, $a = 60\,s^{-1}$, characterized the flames, thus facilitating a chemical kinetic comparison. Pure allene fueled the first flame, and a mixture of 75/25 mol % allene/1-buten-3-yne fueled the second flame, using 1-buten-3-yne as fuel for the first time in counterflow diffusion flames. Comparing the results provided by both instruments showcased agreement within the experimental uncertainty for all species, except for a minimal discrepancy in the case of ethylene. A revised kinetic model [3,13] correctly predicted the experimental trends for most detected species. Notably, adding 1-buten-3-yne decreased benzene while promoting naphthalene formation, highlighting their dependence on the availability of C_3 and C_4 species. This finding and the particular overprediction of 1,3-butadiyne and naphthalene in the C_3+C_4 flame motivated extensive reaction pathway analyses. 1,3-butadiyne impacts naphthalene formation via the $C_4 + 2\,C_3$ pathway [6,7] and by phenyl radical-addition via the $2\,C_3 + C_4$ pathway. Our analysis evidenced both pathways to be responsible for the pronounced increase in naphthalene formation in the C_3+C_4 flame. HACA [27,28] and HAVA [11,15] pathways were found to be of minor effect. In conclusion, we may confirm that 1,3-butadiyne is a critical species in the formation network of naphthalene [1–3,6,7], and using 1-buten-3-yne as fuel places a magnifying glass on these channels. However, the persistent overprediction of 1,3-butadiyne, as seen in previous studies [6,7,14], poses a potential limitation on the accuracy of naphthalene predictions. Future studies should aim to reduce the remaining uncertainties in the rate coefficients of the reactions of C_4H_2 and C_3H_3 from theoretical works [29,30]. Further, we recommend continued investigation of the recombination reaction $C_7H_5 + C_3H_3$ and the highly uncertain but significant oxidation reaction $C_4H_2 + O$. Therefore, the comprehensive speciation dataset provided in the SM will be a unique validation target for kinetic model development, and particularly support C_4 chemistry advancement.

Novelty and significance statement

- This study provides fresh insights into C_4 chemistry by introducing 1-buten-3-yne (C_4H_4) as fuel for the first time in counterflow diffusion flames.
- 1-Buten-3-yne as fuel reduces the complexities usually involved with the formation of unsaturated C_4 species, i.e., fuel-specific reactions in addition to reactions of C_4 species.
- Two flames were investigated targeting specific formation pathways toward naphthalene: one fueled solely with allene and the other with a novel mixture of 75/25 mol% of allene/1-buten-3-yne.
- Opposing trends of benzene and naphthalene at C_4H_4-addition suggest that naphthalene profits from the increased abundance of C_4 species.
- Analyses based on an updated, extensively validated, detailed chemical kinetic model support the conclusion that naphthalene formation depends on $C_4 + 2\,C_3$ and $2\,C_3 + C_4$ pathways.
- The rich speciation datasets from gas chromatography-mass spectrometry and time-of-flight molecular-beam mass spectrometry constitute a unique validation target for future kinetic model development.

CRediT authorship contribution statement

Maximilian Hellmuth: Conceptualization, Experiments, Simulations, Analysis, Writing. **Raymond Langer:** Conceptualization, Simulations, Analysis, Writing. **Anita Meraviglia:** Experiments, Data analysis, Editing. **Joachim Beeckmann:** Reviewing, Editing. **Heinz Pitsch:** Data analysis, Reviewing, Editing, Supervision.

Declaration of competing interest

The authors declare that they have no known competing financial interests or personal relationships that could have appeared to influence the work reported in this paper.

Acknowledgments

This work was funded by the Deutsche Forschungsgemeinschaft (DFG, German Research Foundation) under Germany's Excellence Strategy - Cluster of Excellence 2186 "The Fuel Science Center" - ID: 390919832. Further acknowledgment goes to the financial support from the DFG within the framework of the collaborative research center SFB/Transregio 129 "Oxyflame" (ID: 215035359) and the computing time provided at RWTH Aachen University (project number rwth1433).

Supplementary material

Supplementary material related to this article can be found, in the online version, at https://doi.org/10.1016/j.proci.2024.105620.

References

[1] G. Kukkadapu, S.W. Wagnon, W.J. Pitz, N. Hansen, Identification of the molecular-weight growth reaction network in counterflow flames of the C_3H_4 isomers allene and propyne, Proc. Combust. Inst. 38 (1) (2021) 1477–1485.
[2] N. Hansen, B. Yang, M. Braun-Unkhoff, A. Ramirez, G. Kukkadapu, Molecular-growth pathways in premixed flames of benzene and toluene doped with propyne, Combust. Flame 243 (2022) 112075.
[3] R. Langer, Q. Mao, H. Pitsch, A detailed kinetic model for aromatics formation from small hydrocarbon and gasoline surrogate fuel combustion, Combust. Flame 258 (2023) 112574.
[4] J.A. Miller, S.J. Klippenstein, The recombination of propargyl radicals and other reactions on a C_6H_6 potential, J. Phys. Chem. A 107 (2003) 7783–7799.
[5] S.J. Klippenstein, J.A. Miller, A.W. Jasper, Kinetics of propargyl radical dissociation, J. Phys. Chem. A 119 (2015) 7780–7791.
[6] M. Hellmuth, F. Cameron, S. Faller, L. Schmückert, B. Chen, Y. Ren, H. Pitsch, Synergistic effect on PAH and soot formation in ethylene counterflow diffusion flames by the addition of 1,3-dioxolane - a bio-hybrid fuel, Proc. Combust. Inst. 39 (1) (2023) 899–908.
[7] M. Hellmuth, B. Chen, C. Bariki, L. Cai, F. Cameron, A. Wildenberg, C. Huang, S. Faller, Y. Ren, J. Beeckmann, K. Leonhard, K.A. Heufer, N. Hansen, H. Pitsch, A comparative study on the combustion chemistry of two bio-hybrid fuels: 1,3-dioxane and 1,3-dioxolane, J. Phys. Chem. A 127 (1) (2023) 286–299.
[8] H. Jin, L. Xing, D. Liu, J. Hao, J. Yang, A. Farooq, First aromatic ring formation by the radical-chain reaction of vinylacetylene and propargyl, Combust. Flame 225 (2021) 524–534.
[9] C. Martí, H.A. Michelsen, H.N. Najm, J. Zádor, Comprehensive kinetics on the C_7H_7 potential energy surface under combustion conditions, J. Phys. Chem. A 127 (2023) 1941–1959.
[10] L. Monluc, A.A. Nikolayev, I.A. Medvedkov, V.N. Azyazov, A.N. Morozov, A.M. Mebel, The reaction of *o*-benzyne with vinylacetylene: An unexplored way to produce naphthalene, Chem. Phys. Chem. 23 (2022) e202100758.
[11] A.M. Mebel, A. Landera, R.I. Kaiser, Formation mechanisms of naphthalene and indene: From the interstellar medium to combustion flames, J. Phys. Chem. A 121 (2017) 901–926.
[12] W. Li, J. Yang, L. Zhao, D. Couch, M.S. Marchi, N. Hansen, A.N. Morozov, A.M. Mebel, R.I. Kaiser, Gas-phase preparation of azulene ($C_{10}H_8$) and naphthalene ($C_{10}H_8$) via the reaction of the resonantly stabilized fulvenallenyl ($C_7H_5^{\bullet}$) and propargyl ($C_3H_3^{\bullet}$) radicals, Chem. Sci. 14 (36) (2023) 9795–9805.
[13] R. Langer, Adjoint Sensitivity Analysis for Chemical Kinetic Model Development (Ph.D. thesis), Rheinisch-Westfälische Technische Hochschule Aachen, Aachen, 2023.
[14] W. Pejpichestakul, E. Ranzi, M. Pelucchi, A. Frassoldati, A. Cuoci, A. Parente, T. Faravelli, Examination of a soot model in premixed laminar flames at fuel-rich conditions, Proc. Combust. Inst. 37 (1) (2019) 1013–1021.
[15] R.I. Kaiser, N. Hansen, An aromatic universe–A physical chemistry perspective, J. Phys. Chem. A 125 (18) (2021) 3826–3840.
[16] M. Baroncelli, D. Felsmann, N. Hansen, H. Pitsch, Investigating the effect of oxy-fuel combustion and light coal volatiles interaction: A mass spectrometric study, Combust. Flame 204 (2019) 320–330.
[17] B. Chen, M. Hellmuth, S. Faller, L. May, P. Liu, L. Cai, W.L. Roberts, H. Pitsch, Exploring the combustion chemistry of anisole in laminar counterflow diffusion-flames under oxy-fuel conditions, Combust. Flame 243 (2022) 111929.
[18] C.L. Faiola, M.H. Erickson, V.L. Fricaud, B.T. Jobson, T.M. VanReken, Quantification of biogenic volatile organic compounds with a flame ionization detector using the effective carbon number concept, Atmos. Meas. Tech. 5 (8) (2012) 1911–1923.
[19] J.C. Sternberg, W.S. Gallaway, D.T.L. Jones, The mechanism of response of flame ionization detectors, Gas Chromatogr. (1962) 231–267.
[20] H. Pitsch, R. Langer, FlameMaster v.4.4.0: A C++ computer program for 0D combustion and 1D laminar flame calculations, 2023, https://www.itv.rwth-aachen.de/downloads/flamemaster/.
[21] H. Bufferand, L. Tosatto, B.L. Mantia, M.D. Smooke, A. Gomez, Experimental and computational study of methane counterflow diffusion flames perturbed by trace amounts of either jet fuel or a 6-component surrogate under non-sooting conditions, Combust. Flame 156 (8) (2009) 1594–1603.
[22] S. Dong, S.W. Wagnon, L. Pratali Maffei, G. Kukkadapu, A. Nobili, Q. Mao, M. Pelucchi, L. Cai, K. Zhang, M. Raju, T. Chatterjee, W.J. Pitz, T. Faravelli, H. Pitsch, P.K. Senecal, H.J. Curran, A new detailed kinetic model for surrogate fuels: C3MechV3.3, Appl. Energy Combust. Sci. 9 (2022) 100043.
[23] S. Panigrahy, J. Liang, S.S. Nagaraja, Z. Zuo, G. Kim, S. Dong, G. Kukkadapu, W.J. Pitz, S.S. Vasu, H.J. Curran, A comprehensive experimental and improved kinetic modeling study on the pyrolysis and oxidation of propyne, Proc. Combust. Inst. 38 (2021) 479–488.
[24] Y. Wang, S.H. Chung, Soot formation in laminar counterflow flames, Prog. Energy Combust. Sci. 74 (2019) 152–238.
[25] N. Hansen, J.A. Miller, S.J. Klippenstein, P.R. Westmoreland, K. Kohse-Höinghaus, Exploring formation pathways of aromatic compounds in laboratory-based model flames of aliphatic fuels, Combust. Explos. Shock Waves 48 (5) (2012) 508–515.
[26] L. Zhao, R.I. Kaiser, W. Lu, B. Xu, M. Ahmed, A.N. Morozov, A.M. Mebel, A.H. Howlader, S.F. Wnuk, Molecular mass growth through ring expansion in polycyclic aromatic hydrocarbons via radical–radical reactions, Nature Commun. 10 (2019) 3689.
[27] A.M. Mebel, Y. Georgievskii, A.W. Jasper, S.J. Klippenstein, Temperature- and pressure-dependent rate coefficients for the HACA pathways from benzene to naphthalene, Proc. Combust. Inst. 36 (2017) 919–926.
[28] T.-C. Chu, Z.J. Buras, M.C. Smith, A.B. Uwagwu, W.H. Green, From benzene to naphthalene: Direct measurement of reactions and intermediates of phenyl radicals and acetylene, Phys. Chem. Chem. Phys. 21 (2019) 22248–22258.
[29] G. da Silva, A.J. Trevitt, Chemically activated reactions on the C_7H_5 energy surface: Propargyl + diacetylene, *i*-C_5H_3 + acetylene, and *n*-C_5H_3 + acetylene, Phys. Chem. Chem. Phys. 13 (19) (2011) 8940–8952.
[30] M. Derudi, D. Polino, C. Cavallotti, Toluene and benzyl decomposition mechanisms: Elementary reactions and kinetic simulations, Phys. Chem. Chem. Phys. 13 (48) (2011) 21308–21318.